HNPS Advances in Nuclear Physics

Vol 30 (2024)

HNPS2023

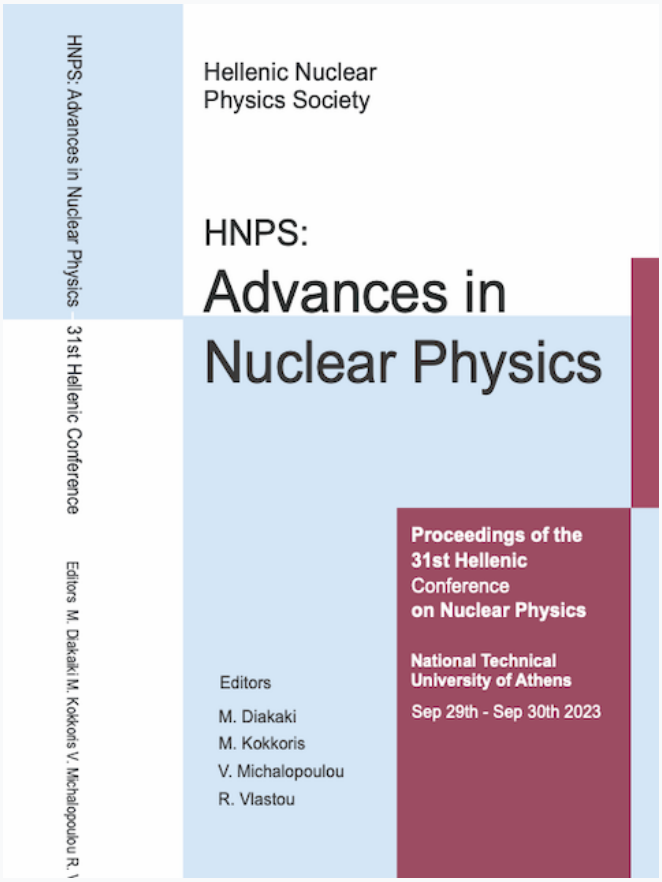

Probing new physics with nuclear recoil data from COHERENT

Dimitrios K. Papoulias

doi: 10.12681/hnpsanp.6290

To cite this article:

Papoulias, D. K. (2024). Probing new physics with nuclear recoil data from COHERENT. *HNPS Advances in Nuclear Physics*, *30*, 81–88. https://doi.org/10.12681/hnpsanp.6290

Probing new physics with nuclear recoil data from COHERENT

D.K. Papoulias*

Department of Physics, National and Kapodistrian University of Athens, Zografou Campus GR-15772, Athens, Greece

Abstract We exploit the full coherent elastic neutrino-nucleus scattering (CEvNS) dataset reported by the COHERENT Collaboration. In particular, we combine the most recent CsI-2021 measurement with the liquid argon (LAr) measurement from the 2020 campaign. In view of the increased statistics, the refined treatment of quenching effects and the better understanding of the error budget, the present study leads to improved constraints for a set of interactions within and beyond the Standard Model (SM). In terms of a dedicated statistical analysis we provide up-to-date limits on the weak mixing angle and the neutron nuclear radius. With respect to beyond the SM phenomena, we improve previous bounds on electromagnetic neutrino properties and novel light mediator scenarios.

Keywords neutrino-nucleus scattering, electroweak parameters, neutrinos beyond the Standard Model

INTRODUCTION

The discovery of neutrino oscillations has brought neutrino physics to a precision era [1,2], characterized by a burgeoning field, expanding experiments, and the proposal of novel detection concepts. Current attention is concentrated towards understanding the role of neutral currents for underpinning aspects of neutrino mass generation [3]. Coherent elastic neutrino-nucleus scattering (CEvNS) experiments [4], and in particular the COHERENT Collaboration, are of instrumental importance in exploring the field. In this study, we analyze the most recent data from the CsI-2021 COHERENT measurement [5], and combine them with the liquid argon (LAr) COHERENT data reported in 2020 [6]. Such detailed study offers a robust and updated analysis of the full COHERENT dataset, providing new insights into conventional electroweak parameters within the Standard Model, such as the weak mixing angle at low momentum transfer, and nuclear physics features [7]. Furthermore, these datasets constitute a prime vehicle to constrain new physics scenarios, including neutrino nonstandard interactions (NSI), neutrino generalized interactions (NGI), light mediators, CP-violating effects, and various neutrino electromagnetic properties, as shown in Ref. [8]. Exploring conversions to sterile neutrinos, induced by oscillations or active-to-sterile transition magnetic moments, is another interesting possibility achievable via CEvNS-based analyses. Moreover, Ref. [9] has gone beyond previous typical analyses, extending the scope to include also new mediators in the up-scattering process by exploring the potential production of a new MeV-scale dark fermion.

Here, we improve previous constraints through a detailed statistical analysis combining the most recent CsI and LAr datasets by addressing experimental details meticulously. Our comprehensive analysis encompasses all relevant uncertainties and detector-specific quantities for both CsI and LAr detectors. For instance, we incorporate efficiency, quenching factor and timing information, along with the relevant systematic uncertainties and all known backgrounds. Whenever relevant, i.e. for the case of CsI detector only, we furthermore include elastic neutrino-electron scattering (EvES) events –which forms another source of background that was previously ignored by similar works– that could mimic a CEvNS signal. Through this careful statistical analysis, our present study aims to address both SM precision tests and new physics scenarios, presenting the most up-to-date constraints. We demonstrate that the inclusion of new CsI data is dramatically improving the sensitivities to the several parameters

* Corresponding author: *dkpapoulias@phys.uoa.gr*

in question, leading to stringent constraints in certain cases and complementing existing bounds from further experimental probes.

RELEVANT CROSS SECTIONS IN THE SM AND BEYOND

The SM differential CEvNS cross section with respect to the nuclear recoil energy $E_{\rm nr}$ reads

$$\frac{d\sigma}{dE_{nr}}\Big|^{SM}_{CEvNS} = \frac{G_F^2 m_N}{\pi}(Q_V^{SM})^2\left(1-\frac{m_N E_{nr}}{2E_\nu^2}\right)F_W^2(|\vec{q}|^2), \quad (1)$$

where G_F, E_ν, m_N denote the Fermi's constant, incident neutrino energy and nuclear mass respectively. In the above expression the weak nuclear charge reads

$$Q_V^{\rm SM} = g_V^p Z + g_V^n N = \frac{1}{2}(1-4\,sin^2\theta_W)Z - \frac{1}{2}N, \quad (2)$$

where Z, N refer to the number of protons and neutrons within the nucleus $\mathcal{N}(A,N)$. The nuclear form factor incorporates the information of coherency loss due to the finite nuclear size and takes the form

$$F_W^2(|\vec{q}|^2) = \frac{3j_1(|\vec{q}|R_A)}{|\vec{q}|R_A}\left(\frac{1}{1+|\vec{q}|^2 a_k^2}\right), \quad (3)$$

with j_1, R_A, and $\vec{q}$ being the 1st-order spherical Bessel function, the nuclear radius, and the three-momentum transfer, respectively, while $a_k = 0.7$ fm. The corresponding EvES differential cross section with respect to the electron recoil energy $E_{\rm er}$ in the SM reads

$$\frac{d\sigma}{dE_{\rm er}}\Big|^{\rm SM}_{\rm EvES} = \mathcal{Z}^{\mathcal{N}}_{\rm eff}\frac{G_F^2 m_e}{2\pi}[(g_V^a+g_A^a)^2+(g_V^a-g_A^a)^2\left(1-\frac{E_{\rm er}}{E_\nu}\right)-([g_V^a]^2-[g_A^a]^2)\frac{m_e E_{\rm er}}{E_\nu^2}], \quad (4)$$

where m_e denotes the mass of the electron, while the corresponding flavor-dependent vector and axial vector couplings are defined as $g_V^a = 2sin^2\theta_W - \frac{1}{2} + \delta_{ae}$ and $g_A^a = -\frac{1}{2} + \delta_{ae}$, $a = e,\mu,\tau$. Notice that the Kronecker δ is introduced to account for the fact that for of $\nu_e - e$ scatetring both charged- and neutral-currents contribute to the EvES scattering amplitude, unlike the $\nu_\mu - e, \nu_\tau - e$ cases where only neutral-currents are relevant. When antineutrinos are involved the following substitution is required: $g_A^a \to -g_A^a$. Finally, we also take into account that the electrons in the detector material of COHERENT experiment are not free but bound within the atomic nucleus $\mathcal{N}(A,N)$. For this reason the quantity $\mathcal{Z}^{\mathcal{N}}_{\rm eff}$ is introduced in the cross section and represents the effective number of protons seen by the neutrinos, for an energy deposition $E_{\rm er}$. The effective charges for CsI and Ar are taken from Ref.[10].

Turning our attention to electromagnetic contributions, the corresponding CEvNS and EvES differential cross sections can be cast in the form

$$\frac{d\sigma}{dE_{\rm nr}}\Big|^{\rm mag}_{\rm CEvNS} = \frac{\pi\alpha_{\rm EM}^2}{m_e^2}\left(\frac{1}{E_{\rm nr}}-\frac{1}{E_\nu}\right)Z^2F_W^2(|\vec{q}|^2)\left(\frac{\mu_\nu}{\mu_B}\right)^2, \quad (5)$$

for CEvNS and

$$\frac{d\sigma}{dE_{\rm er}}\Big|^{\rm mag}_{\rm EvES} = \mathcal{Z}^{\mathcal{N}}_{\rm eff}\frac{\pi\alpha_{\rm EM}^2}{m_e^2}\left(\frac{1}{E_{\rm er}}-\frac{1}{E_\nu}\right)\left(\frac{\mu_\nu}{\mu_B}\right)^2, \quad (6)$$

for EvES. In the above expressions a_{EM} refers to the fine-structure constant and μ_ν to neutrino magnetic moment. Another intriguing electromagnetic property of neutrinos that can be investigated in low-energy neutrino scattering experiments is the potential existence of a minute neutrino electric charge (EC), often termed the neutrino millicharge. In present, its impact to the SM cross sections can be obtained via the shifts $g_V^p \to g_V^p - Q^{\rm EC}$ for CEvNS and $g_V^a \to g_V^a + Q^{\rm EC}$ for EvES where the quantity $Q^{\rm EC}$ is expressed according to [8]

$$Q^{\rm EC} = 2\sqrt{2}\pi\frac{\alpha_{\rm EM}}{G_F q^2}q_\nu, \quad (7)$$

where q_ν is the neutrino millicharge ($q^2 = -2\,m_i E_{ir}$ is the four momentum transfer for i = n,e).

Next we explore new potential contributions to the SM cross sections which arise in the presence

of novel light mediators in the framework of extra $U(1)$ symmetries. In this study we consider both vector- (V) and scalar-type (S) neutral mediators, with mass m_V and m_S, respectively. In this case the CEvNS cross section can be expressed in terms of the SM cross section given in Eq.(1), as

$$\frac{d\sigma}{dE_{\rm nr}}\Big|^{V}_{\rm CEvNS} = \left(1+\frac{3(N+Z)g_V^2}{\sqrt{2}G_F\,Q_V^{\rm SM}\,(2m_N E_{\rm nr}+m_V^2)}\right)^2 \frac{d\sigma}{dE_{\rm nr}}\Big|^{\rm SM}_{\rm CEvNS}, \tag{8}$$

while for EvES the new cross section is simply taken from Eq.(2) and the substitution

$$g_V^a \to g_V^a + \frac{g_V^2}{2\sqrt{2}G_F\,(2m_e E_{\rm er}+m_V^2)}\,, \tag{9}$$

where g_V is the new coupling. In the same vein, the corresponding expressions for the case of a scalar mediator are given as follows

$$\frac{d\sigma}{dE_{\rm nr}}\Big|^{S}_{\rm CEvNS} = \frac{m_N^2 E_{\rm nr}\,C_S^2}{4\pi E_\nu^2 (2m_N E_{\rm nr}+m_S^2)^2} F_W^2(|\vec{q}|^2), \tag{10}$$

with the corresponding scalar charge written as

$$C_S \approx (14\,(N+Z)+1.1Z)g_S^2, \tag{11}$$

for the case of CEvNS. For the case of EvES the respective cross section takes the form

$$\frac{d\sigma}{dE_{\rm er}}\Big|^{S}_{\rm EvES} = \mathcal{Z}_{\rm eff}^{\mathcal{N}}\,\frac{m_e^2 E_{\rm er}\,g_S^4}{4\pi E_\nu^2 (2m_e E_{\rm er}+m_S^2)^2}. \tag{12}$$

STATISTICAL ANALYSIS

We calculate the number of expected events at the CsI and LAr detectors taking into account all relevant detector-specific quantities. For the CsI detector, the number of events in the i-th bin can be evaluated as [7,9]

$$N_i^{\rm CEvNS,\mathcal{N}} = N_{\rm target}\int_{E_{\rm nr}^i}^{E_{\rm nr}^{i+1}} dE_{\rm nr}\,\varepsilon_E(E_{\rm nr})\int_0^{E'^{\rm max}_{\rm nr}} dE'_{\rm nr}\,P(E_{\rm nr},E'_{\rm nr})\times$$
$$\int_{E_\nu^{\rm min}(E'_{\rm nr})}^{E_\nu^{\rm max}} dE_\nu \sum_{x=\nu_e,\nu_\mu,\bar{\nu}_\mu}\frac{d\Phi_x}{dE_\nu}(E_\nu)\,\frac{d\sigma}{dE_{\rm nr}}\Big|^{\kappa}_{\rm CEvNS}(E_\nu,E'_{\rm nr})\,. \tag{13}$$

Here, ε_E and P stand for the efficiency in energy reconstruction and the resolution of the CsI or LAr detectors, taken from Refs. [5,6]. Moreover $E_{\rm nr}, E'_{\rm nr}$ stand for the reconstructed and true nuclear recoil energies, $\frac{d\Phi_x}{dE_\nu}$ denotes the neutrino energy distributions at the Spallation Neutron Source, $N_{\rm target}$ is the number of target nuclei and finally κ refers to the different interaction cross sections discussed in the previous section. The integration limits can be trivially obtained from the kinematics of the process. The nuclear recoil spectrum obtained from Eq.(13) is then converted to an electron recoil spectrum via the quenching factor as given by the COHERENT Collaboration (see Refs. [5,6]). For the case of CsI detector, the electron recoil spectrum is further converted to a photoelectron spectrum.

In the next step of our simulation procedure we compute the time-dependent spectra at COHERENT, for both CsI and LAr detectors. This is done by weighting the binned events in energy space with the corresponding time distribution of the incoming neutrinos, denoted here by $f_T^x(t_{\rm rec})$, where $t_{\rm rec}$ is the reconstructed time as measured by COHERENT. Then, the number of events in the i-th energy bin and j-th time bin is calculated as [7,9]

$$N_{i,j}^{\rm CEvNS,\mathcal{N}} = \sum_{x=\nu_e,\nu_\mu,\bar{\nu}_\mu}\int_{t_{\rm rec}^j}^{t_{\rm rec}^{j+1}} dt_{\rm rec}\,\varepsilon_T(t_{\rm rec})f_T^x(t_{\rm rec})N_{i,x}^{\rm CEvNS,\mathcal{N}}, \tag{14}$$

where $\varepsilon_T(t_{\rm rec})$ is the efficiency in time reconstruction. The EvES events are calculated in a completely analogous way as for the CEvNS case, with the only difference being the obvious fact that there is no

need to correct for the quenching factor. In what follows we perform a statistical analysis, taking into account the various background components and all relevant systematic uncertainties following the procedure detailed in Ref. [7].

RESULTS AND DISCUSSION

We first calculate the expected number of events for the CsI detector and compare our results against the experimental data reported by the 2021 measurement of COHERENT (for the case of LAr detector, the corresponding results will be presented elsewhere). The calculated 2D spectrum, binned in both energy and time, is illustrated in Fig.1. It is interesting to notice that a better agreement with the experimental data is obtained when all uncertainties are taken into account (orange histograms) in comparison to the case of the bare calculation of the theoretical spectra without accounting for any uncertainties (cyan histograms). This constitutes an important justification of our calculated spectra, and thus we are now in position to explore the effects of SM uncertainties due to the weak mixing angle and nuclear physics, to which we now turn.

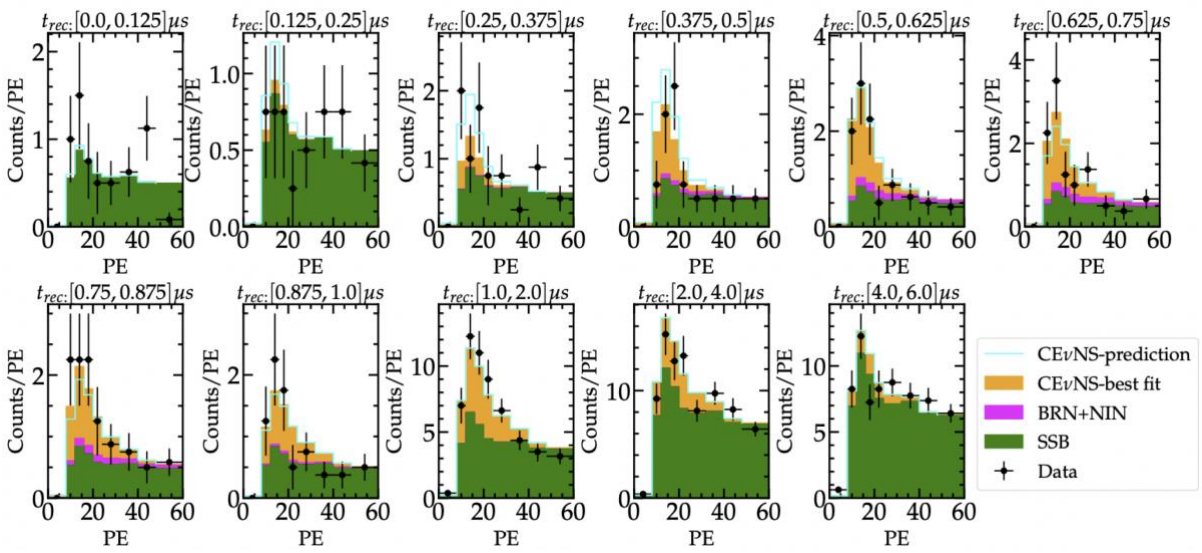

Figure 1. *2D spectra in the SM for the CsI detector where all backgrounds are taken into account and a comparison with the experimental data is given [7]*

In the left panel of Fig. 2 we present the $\Delta\chi^2$ profile obtained from the analysis of CsI (magenta), LAr (orange) and the combined CsI+LAr (blue) data as a function of the weak mixing angle $\sin^2\theta_w$. The combined fit of CsI+LAr data leads to the following best fit value for this parameter at 1σ: $\sin^2\theta_w = 0.237 \pm 0.029$. As can be seen from the plot, clearly the result is mainly driven by the recent CsI data. We note that for this analysis the EvES events on CsI can be safely neglected. The right panel of Fig. 2 shows the $\sin^2\theta_w$ RGE evolution in the SM (light red line), calculated in the MS renormalization scheme, together with our combined CsI+LAr determination (blue) and other measurements at different scale. It is interesting to note that the full COHERENT data provide a determination of the weak mixing angle at low-energies, in a region where other data-driven constraints are absent.

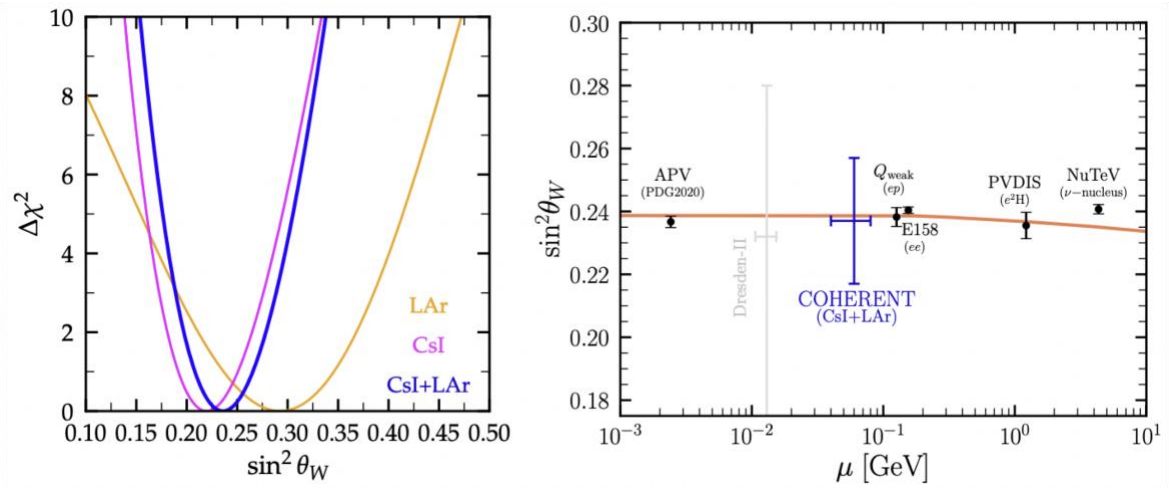

Figure 2. *$\Delta\chi^2$ profiles of the determination of the weak mixing angle using COHERENT data (left). Comparison across different energies with other known constraints (right) [7].*

In the left panel of Fig. 3 we display the sensitivity on the neutron RMS radius, R_n, of argon and CsI obtained from the analysis of COHERENT data. For the case of LAr, here we have updated the result on R_n(Ar) obtained in a previous work [11], using not only the energy data but also the timing information and the various shape uncertainties described in Ref. [7]. The 1σ regions on the neutron RMS radii of argon and CsI from our analysis are $R_n(\mathrm{Ar}) \in [0.00, 3.72]$ fm and $R_n(\mathrm{CsI}) \in [5.22, 6.03]$ fm. For completeness, in the right panel of Fig. 3 we also present the allowed regions in the space of the two unknown SM parameters $(R_n, \sin^2\theta_w)$. As can be seen, the latter are still poorly constrained, thus calling for a better determination of the nuclear uncertainties in the spirit of a nuclear structure model.

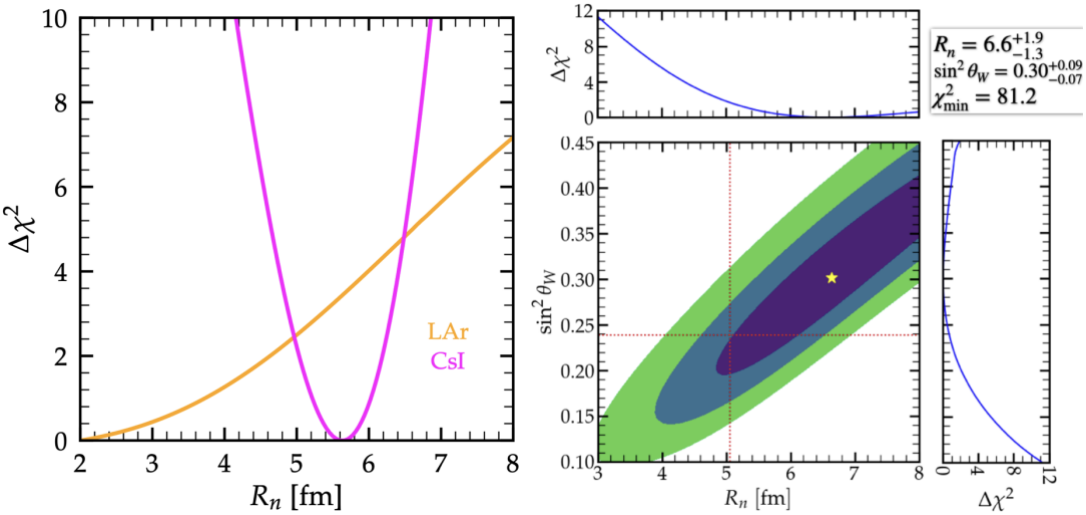

Figure 3. *Sensitivity on the neutron RMS radii of argon and CsI (left) [7]. Combined analysis assuming both the weak mixing angle and the RMS neutron radius of CsI as free parameters (right).*

The constraints on neutrino effective magnetic moment μ_{ν_e}, μ_{ν_μ} are summarized in Fig. 4. In the left (middle) panel, we present the $\Delta\chi^2$ profiles as a function of the effective electron neutrino (muon neutrino) magnetic moment. We assume that only one magnetic moment is nonzero at a time, and we include EvES events in the CsI analysis. One finds an improvement of a factor ∼ 2 with the recent CsI data in comparison to the LAr data set. From the combined analysis of CsI+LAr data, at 90% C.L. we

find the upper limits: $\mu_{\nu_e} < 3.6\ (3.8) \times 10^{-9}\ \mu_B$ and $\mu_{\nu_\mu} < 2.4\ (2.6) \times 10^{-9}\ \mu_B$, where the limits in parenthesis indicate the results from the CEvNS-only analysis. We have also performed a combined analysis, allowing both effective MM to vary simultaneously. The corresponding result is presented in the right panel of Fig. 4. We find that there is a tiny part of the region allowed in the combined analysis which falls outside the CsI-driven contour. This is due to the fact that the analysis of LAr data leads to a nonzero best fit coupling, in contrast to the CsI data (see left and middle panels).

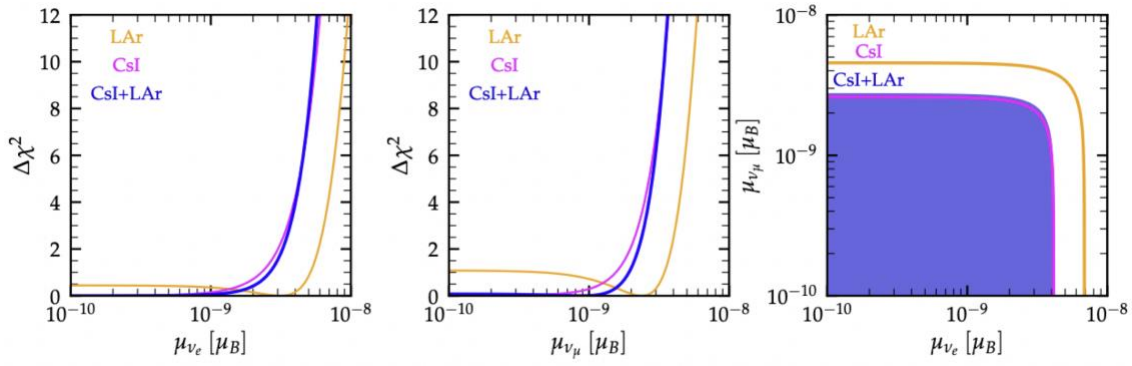

Figure 4. *Left and middle panels: $\Delta\chi^2$ profile for the effective neutrino magnetic moments obtained from the analysis of CsI (magenta), LAr (orange) and CsI + LAr (blue) data. Right panel: 90% C.L. allowed regions when two effective magnetic moments are taken simultaneously. The analysis of CsI data includes CEvNS + EvES interactions [7].*

The $\Delta\chi^2$ profile for the neutrino electric charge (EC) parameters $q_{\nu_{ee}}$ and $q_{\nu_{\mu\mu}}$ is given in the upper-left and upper-middle plots of Fig. 5. The upper-right plot shows the 90% C.L. (2 d.o.f.) allowed regions in the plane ($q_{\nu_{ee}}$, $q_{\nu_{\mu\mu}}$), when both parameters are allowed to vary simultaneously. From the combined analysis of CsI+LAr data, we find the following 1σ allowed intervals are in the 10^{-8}e ballpark. Note that, since in EvES the momentum transferred is much smaller than in CEvNS interactions, the inclusion of EvES events in the analysis strongly enhances the sensitivity of COHERENT data to neutrino EC. This is shown in the lower panels of Fig. 5, where a dramatic improvement of two orders or magnitude is gained when including EvES events.

We finally focus on novel mediators and we present in Fig. 6 the 90% C.L. (2 d.o.f.) exclusion regions for the universal light vector model (left) and scalar scenario (right), where the dark blue curves demonstrate the result from our combined CsI+LAr analysis. In order to make a comparison with the available constraints from other experimental probes, we compare our results with the existing limits from other CEvNS experiments, in particular CONNIE, CONUS and Dresden-II. We superimpose the results coming from dark matter direct detection experiments (XENONnT and LZ) and from Borexino, in all cases assuming solar neutrinos. We also show the results from collider and beam dump experiments. For completeness in the low mass regime, we illustrate the bound from Big Bang Nucleosynthesis (BBN) obtained by requiring that the nonstandard mediator couples to neutrinos only, as well as the 2σ preferred region to account for the muon anomalous magnetic moment $(g-2)_\mu$.

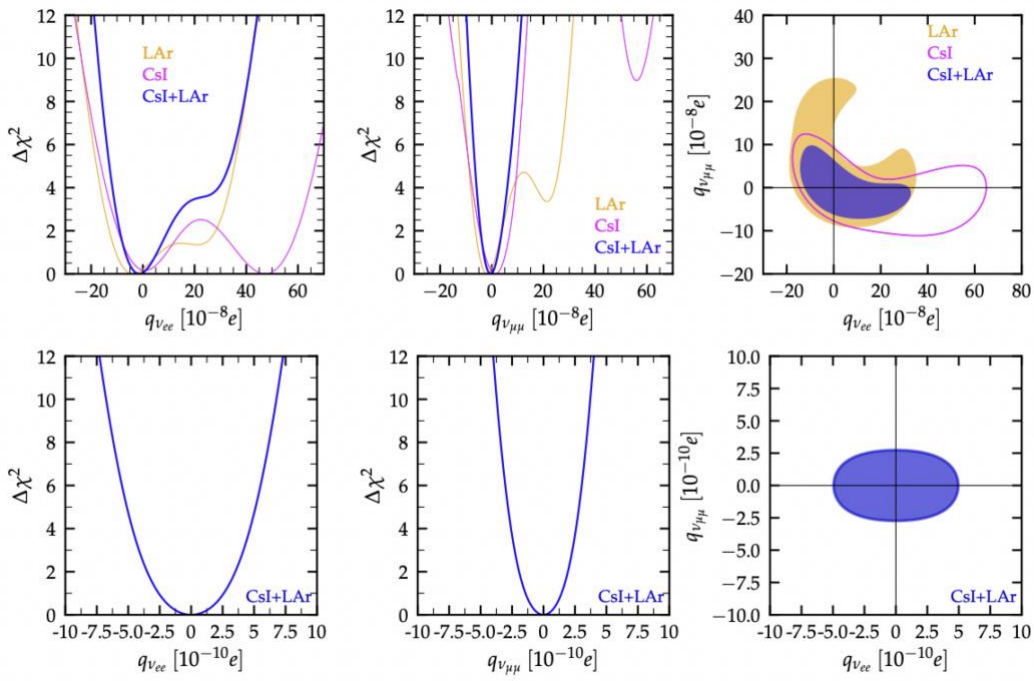

Figure 5. *Left and middle panels: $\Delta\chi^2$ profile for the neutrino electric charges obtained from the analysis of CsI (magenta), LAr (orange) and CsI + LAr (blue) data. Right panels: 90% C.L. (2 dofs) allowed regions for the neutrino electric charges, in units of the elementary charge e. In the upper (lower) panels the analysis of CsI data includes only CEvNS (CEvNS+EvESS) interactions [7].*

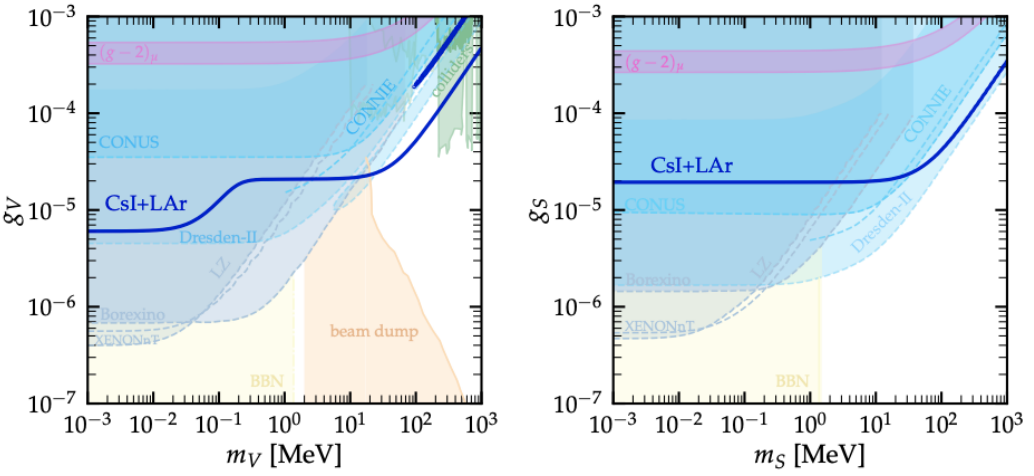

Figure 6. *90% C.L. exclusion regions for novel vector (left) and scalar (right) mediators. A comparison with various limits in the literature is also given [7].*

CONCLUSIONS

In this paper we have analyzed the updated CsI data release from the COHERENT experiment and combined this result with the previous LAr dataset in an effort to infer constraints for a set of interesting parameters within the SM and beyond. By performing a thorough statistical analysis including all systematic errors plus the relevant nuisance parameters associated to signal shape uncertainties, we have probed SM parameters such as the weak mixing angle and nuclear physics. Concerning physics beyond the SM we have concentrated on electromagnetic neutrino properties, namely the neutrino magnetic moment and neutrino millicharges. We have finally presented the 90% C.L. exclusion regions on the relevant coupling and mass for the case of novel light mediators. Specifically, we have presented

two characteristic such examples assuming vector- and scalar-type interactions. In all cases, we conclude that the inclusion of the recent CsI data significantly improves the CEvNS sensitivity in most of these physics cases. Furthermore, we find that the inclusion of EvES events in the expected signal at the CsI detector has led to even better constraints, especially for the cases where the recoil energy has an inversely proportional dependence in the differential cross sections.

Acknowledgments

The author wishes to thank his collaborators in Ref. [7,9]. This work was supported by the Hellenic Foundation for Research and Innovation (H.F.R.I.) under the "3rd Call for H.F.R.I. Research Projects to support Post-Doctoral Researchers" (Project Number: 7036).

References

[1] T. Kajita, Rev. Mod. Phys. 88, 030501 (2016)
[2] A.B. McDonald, Rev. Mod. Phys. 88, 030502 (2016)
[3] J. Schechter and J. Valle, Phys. Rev. D 22, 2227 (1980)
[4] M. Abdullah et al., Snowmass 202.xwx
[5] D. Akimov et al. [COHERENT Collaboration], Phys. Rev. Lett. 129, 081801 (2022)
[6] D. Akimov et al. [COHERENT Collaboration], Phys. Rev. Lett. 126, 012002 (2021)
[7] V. De Romeri et al., JHEP 04, 035 (2023)
[8] M. Atzori Corona et al., JHEP 09, 164 (2022)
[9] P.M. Candela, V. De Romeri, D.K. Papoulias, Phys. Rev. D 108, 055001 (2023).
[10] A. Thompson et al., X-ray data booklet (2009); url: https://xdb.lbl.gov/
[11] O. Miranda et al., JHEP 05, 130 (2020)